Disturbance Rejection and Control System Design Based on an Improved Equivalent-Input-Disturbance Approach

Qicheng Mei, Jinhua She, *Fellow, IEEE*, Feng Wang, *Member, IEEE*, and Yosuke Nakanishi, *Member, IEEE*

***Abstract*—This article presents an improved equivalent-input-disturbance (EID) approach to actively rejecting exogenous disturbances for a plant. A control system based on the approach includes a new EID estimator constructed by embedding integrals to the conventional EID estimator. These integrals enable the estimator to improve the disturbance-estimation precision without amplifying the effect of measurement noise. Stability conditions of the control system are obtained using separation theorem. The system design ensures that the control system satisfies the stability conditions. Experiments of a rotational control system demonstrate the validity of the approach.**

***Index Terms*—Disturbance rejection, equivalent-input-disturbance (EID), integrals.**

I. Introduction

DISTURBANCE rejection is a fundamental issue in designing a control system [1]. Active-disturbance-rejection (ADR) methods, such as disturbance-observer-based (DOB) method [2], [3], active-disturbance-rejection-control method [4], and generalized-extended-state-observer (GESO) method [5] have been widely used to reject disturbances because they solved the tradeoff problem between the sensitivity and complementary sensitivity of the one-degree-of-freedom control system [6].

The equivalent-input-disturbance (EID) approach [7], [8] is one of the ADR methods. It focuses on the effect of disturbances on the output of a plant rather than the disturbances themselves. In the approach, the effect is observed by a Luenberger observer. Then, an EID estimator generates a control signal using the state-observation error. This signal has the same effect on the output as the disturbances do, and is called an EID. The approach takes the EID into the control input channel that directly compensates for the effect of the disturbances. Moreover, since the EID approach requires neither the inverse dynamics of a plant nor the differentiability of the disturbances, it has been successfully applied to servo systems [9], [10], uncertain systems [11], [12], time-delay systems [13], [14], and nonlinear systems [15], [16].

Note that the EID approach does not contain an internal model of a disturbance. It cannot completely reject the disturbance in steady state [17]. Thus, there is room for improving the disturbance-rejection performance. Considering that the EID is generated using the state-observation error, researchers modified the observer for further improving disturbance-rejection performance. For example, a sliding-mode observer [18], a proportional-integral observer (PIO) [19], and a high-gain observer [20] were used to replace the Luenberger observer to improve the state-estimation accuracy. However, the sliding-mode observer causes system chattering; the state convergence speed of the PIO is slow; and the high-gain observer causes the spike phenomenon. In addition, there are studies modifying the EID estimator. Mei *et al.* [21] used a {1} inverse of the input matrix in the estimator. Yu *et al.* [22] added a gain matrix in the estimator. Both of them provided freedom to adjust the performance. Wang *et al.* [23] added a mechanism to adaptive adjust the gain matrix. Du *et al.* [24] added a stable zero to compensate for the phase lag of the EID estimator. While they improve the disturbance-rejection performance, they amplify the effect of measurement noise.

Different from the above studies, we developed an improved EID approach (IEID) to improve the disturbance-rejection performance. First, we explained the limitation of the conventional EID estimator. Next, we constructed an IEID-based control system, which embedded integrals in the conventional EID estimator to remove the limitation. Then, we investigated the

Manuscript received 28 November 2021; revised 6 March 2022; accepted 1 April 2022. Date of publication 29 April 2022; date of current version 16 November 2022. This work was supported in part by the National Natural Science Foundation of China under Grants 61873348 and 62106240; in part by the Natural Science Foundation of Hubei Province, China, under Grant 2020CFA031; in part by the Wuhan Applied Foundational Frontier Project under Grant 2020010601012175; in part by the 111 Project under Grant B17040; and in part by the JSPS KAKENHI under Grant 22H03998. *(Corresponding author: Jinhua She.)*

Qicheng Mei and Feng Wang are with the School of Automation, China University of Geosciences, Wuhan 430074, China, with the Hubei Key Laboratory of Advanced Control and Intelligent Automation for Complex Systems, Wuhan 430074, China, and also with the Engineering Research Center of Intelligent Technology for Geo-Exploration, Ministry of Education, Wuhan 430074, China (e-mail: meiqicheng@cug.edu.cn; wangfeng@cug.edu.cn).

Jinhua She is with the School of Engineering, Tokyo University of Technology, Hachioji 192-0982, Japan (e-mail: she@stf.teu.ac.jp).

Yosuke Nakanishi is with the Graduate School of Environment and Energy Engineering, Waseda University, Shinjuku-ku 169-8555, Japan (e-mail: nakanishi-yosuke@waseda.jp).

Color versions of one or more figures in this article are available at https://doi.org/10.1109/TIE.2022.3169843.

Digital Object Identifier 10.1109/TIE.2022.3169843

stability of the control system and designed the gains of the integrals based on the frequency-domain performance index. Finally, we applied the IEID approach to a rotational-speed-control system. Experiments of this system demonstrated the validity of the approach. The main contributions of this study are as follows.

1) We developed an IEID estimator that contains a proportional-integral (PI) chain to enhance the disturbance-rejection performance.
2) We devised an algorithm based on a phase-margin index to design the IEID estimator, which makes the IEID-based control system have both satisfied disturbance-rejection and noise-suppression performance.
3) We analyzed the disturbance-rejection mechanism of the IEID approach and used a rotational-speed-control system to exhibit its superiors over the EID approach, the DOB approach, and the GESO approach in rejecting disturbances.

In this article, $\mathbb{R}^k$ is a set of k-dimensional column vectors; $\mathbb{R}^{k\times m}$ is a set of $k \times m$ real matrices; I stands for an identity matrix; and $X(s)$ is the Laplace transform of $x(t)$. For a transfer function $G(s)$, there is $\|G\|_\infty := \sup_{0\le\omega<\infty} \sigma_{\max}[G(j\omega)]$ and $\|G(j\omega)\| := \sigma_{\max}[G(j\omega)]$, where $\sigma_{\max}[G(j\omega)]$ is the maximum singular value of $G(j\omega)$ at the frequency ω.

II. Problem Formulation

Consider a minimum-phase plant with an exogenous disturbance

$$\begin{cases} \dot{x}_p(t) = Ax_p(t) + Bu(t) + B_d d(t) \\ y_p(t) = Cx_p(t) \end{cases} \tag{1}$$

where $x_p(t)$ $(\in \mathbb{R}^k)$ is the state; $u(t)$ $(\in \mathbb{R})$ is the control input; $y_p(t)$ $(\in \mathbb{R})$ is the output; $d(t)$ $(\in \mathbb{R}^{k_d})$ is the exogenous disturbance; and A $(\in \mathbb{R}^{k\times k})$, B $(\in \mathbb{R}^{k\times 1})$, B_d $(\in \mathbb{R}^{k\times k_d})$, and C $(\in \mathbb{R}^{1\times k})$ are constant matrices. If the disturbance is unmatched, B and B_d have different dimensions.

We make two assumptions for the plant (1):

Assumption 1: It is controllable and observable.

Assumption 2: It has no zeros on the imaginary axis.

Assumptions 1 and 2 ensure that there exists an EID, $d_e(t)$ $(\in \mathbb{R})$, on the control input channel that has the same effect on the output as $d(t)$ does [25]. Thus, we can rewrite plant (1) to be

$$\begin{cases} \dot{x}(t) = Ax(t) + B[u(t) + d_e(t)] \\ y(t) = Cx(t) \end{cases} \tag{2}$$

where $x(t)$ $(\in \mathbb{R}^k)$ is the state and $y(t)$ $(\in \mathbb{R})$ is the output of the plant (2). In the rest of this article, we use plant (2) as the model of the plant (1) for analysis.

The conventional EID approach uses the mechanism (Fig. 1) to reject $d_e(t)$ [8]. The state observer in it is

$$\begin{cases} \dot{\hat{x}}(t) = A\hat{x}(t) + Bu_f(t) + L[y(t) - C\hat{x}(t)] \\ \hat{y}(t) = C\hat{x}(t) \end{cases} \tag{3}$$

where $\hat{x}(t)$ is the state of the observer, $\hat{y}(t)$ is the output, L is the observer gain, and $u_f(t)$ is the feedback input. Setting

$$\Delta x(t) = \hat{x}(t) - x(t) \tag{4}$$

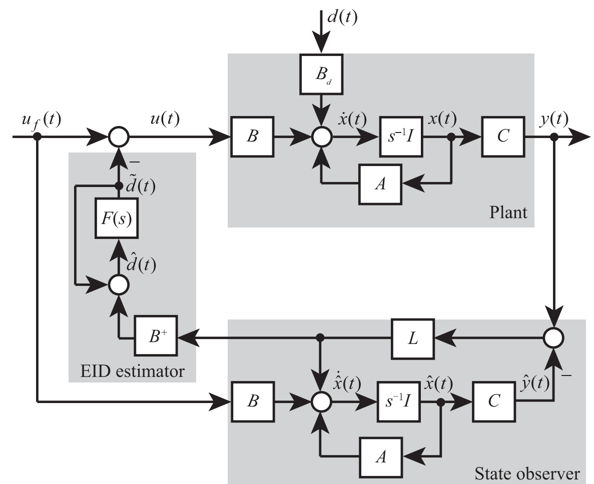

Fig. 1. Disturbance-rejection mechanism of the EID approach.

the EID approach gives an estimated EID [7]

$$\hat{d}(t) = -B^+LC\Delta x(t) + u_f(t) - u(t) \tag{5}$$

where $B^+ = (B^{\mathrm{T}}B)^{-1}B^{\mathrm{T}}$ is a Moore–Penrose inverse of B. To select a frequency band of disturbance rejection, $\hat{d}(t)$ is filtered by a first-order low-pass filter

$$F(s) = \frac{1}{Ts+1} \tag{6}$$

where T is the time constant and chosen to be

$$T = \frac{1}{3\sim 5}\frac{1}{\omega_r} \tag{7}$$

where ω_r is the highest angular frequency for the disturbance. The filtered $\hat{d}(t)$ is $\tilde{d}(t)$, which satisfies

$$\tilde{D}(s) = F(s)\hat{D}(s). \tag{8}$$

Incorporating $\tilde{d}(t)$ into the control input channel yields a control law

$$u(t) = u_f(t) - \tilde{d}(t). \tag{9}$$

For analyzing the disturbance-rejection performance of the mechanism, we combine (2), (3), (4), and (9), which yields

$$\Delta\dot{x}(t) = (A - LC)\Delta x(t) + B[\tilde{d}(t) - d_e(t)]. \tag{10}$$

According to (5), (6), (8), and (9), we obtain

$$\tilde{D}(s) = -\frac{1}{Ts}B^+LC\Delta X(s). \tag{11}$$

Redrawing Fig. 1 based on (2), (10), and (11) yields Fig. 2, in which

$$P(s) = C(sI - A)^{-1}B \tag{12}$$

$$N(s) = -[sI - (A - LC)]^{-1}B \tag{13}$$

$$G_c(s) = \left[1 - \frac{1}{Ts}B^+LCN(s)\right]^{-1}. \tag{14}$$

Fig. 2 shows that the EID-based control system inserts a transfer function, $G_c(s)$, into the plant (2). If there is $\|G_c\|_\infty \approx 0$, then $d_e(t)$ is almost rejected.

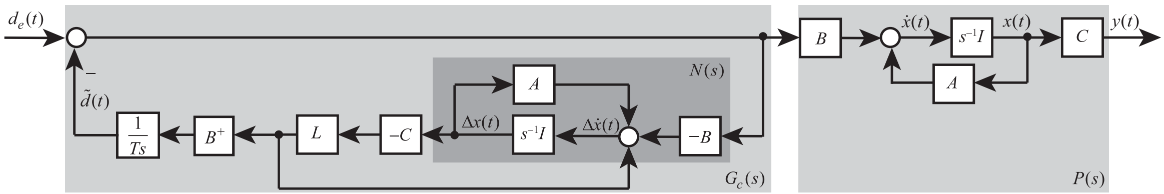

Fig. 2. Simplification of Fig. 1.

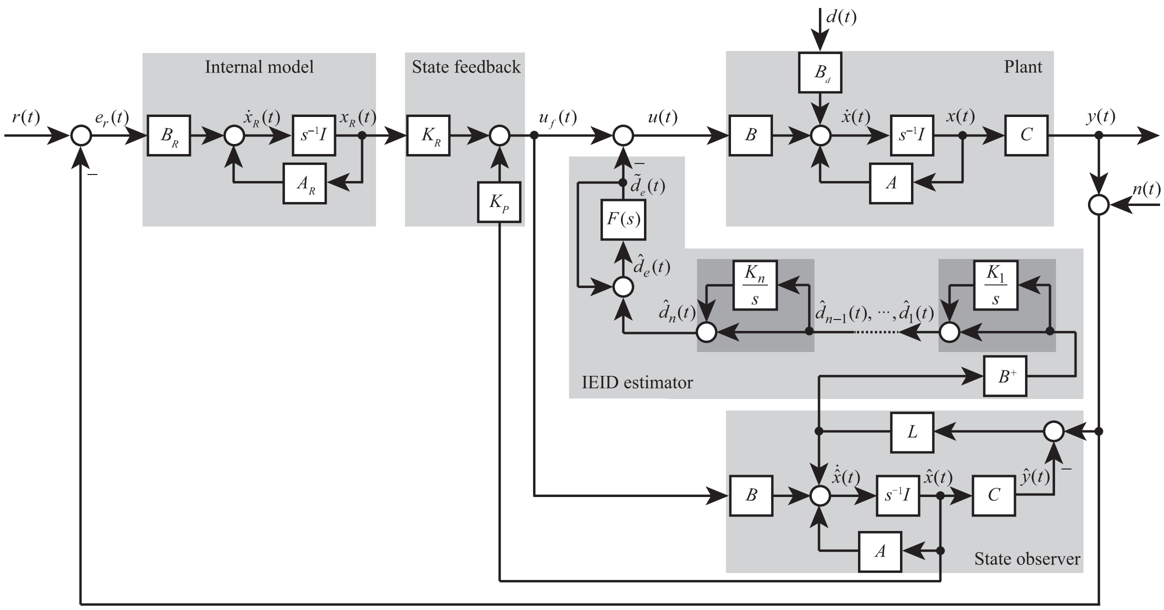

Fig. 3. Configuration of an IEID-based control system.

The conventional EID approach designs an observer gain, L, that ensures $\|N\|_\infty \approx 0$. Thus, (14) can be rewritten to be

$$G_c(s) = \left\{1 - \frac{1}{Ts}[B^+(sI - A)N(s) - 1]\right\}^{-1} \approx \frac{Ts}{Ts+1}. \tag{15}$$

Note that only a small enough T can ensure $\|G_c\|_\infty \approx 0$. However, this T inevitably amplifies measurement noise.

III. System Configuration and Stability Analysis

In this section, we first construct an IEID-based control system (Fig. 3) that solves the above problem of the conventional EID approach. Then, we analyze the stability of the control system.

A. Configuration of IEID-Based Control System

The IEID-based control system has the following five parts:

1) the plant;
2) an internal model;
3) a state observer;
4) an IEID estimator;
5) a state-feedback controller.

The internal model of the reference input, $r(t)$ $(\in \mathbb{R})$, is

$$\dot{x}_R(t) = A_R x_R(t) + B_R e_r(t) \tag{16}$$

where $e_r(t) = r(t) - y(t)$ is the reference-tracking error, $x_R(t)$ $(\in \mathbb{R}^r)$ is the state, A_R $(\in \mathbb{R}^{r\times r})$ is the system matrix, and B_R $(\in \mathbb{R}^{r\times 1})$ is the input matrix of the internal model. It is designed to guarantee the steady-state reference-tracking performance.

In the IEID estimator, there are n newly embedded integrals, which construct n proportional-integral (PI) links. The output of each PI link is

$$\hat{d}_1(t) = -B^+LC\left[\Delta x(t) + K_1\int_0^t \Delta x(t)\mathrm{d}t\right] \tag{17}$$

$$\hat{d}_2(t) = \hat{d}_1(t) + K_2\int_0^t \hat{d}_1(t)\mathrm{d}t \tag{18}$$

$$\cdots$$

$$\hat{d}_n(t) = \hat{d}_{n-1}(t) + K_n\int_0^t \hat{d}_{n-1}(t)\mathrm{d}t \tag{19}$$

where $K_1, K_2, \ldots, K_n$ are the gains of the integrals. We assume that they satisfy

$$K_1 \leq K_2 \leq \cdots \leq K_n. \tag{20}$$

A new estimated EID generated by the IEID estimator is

$$\hat{d}_e(t) = \hat{d}_n(t) + u_f(t) - u(t). \tag{21}$$

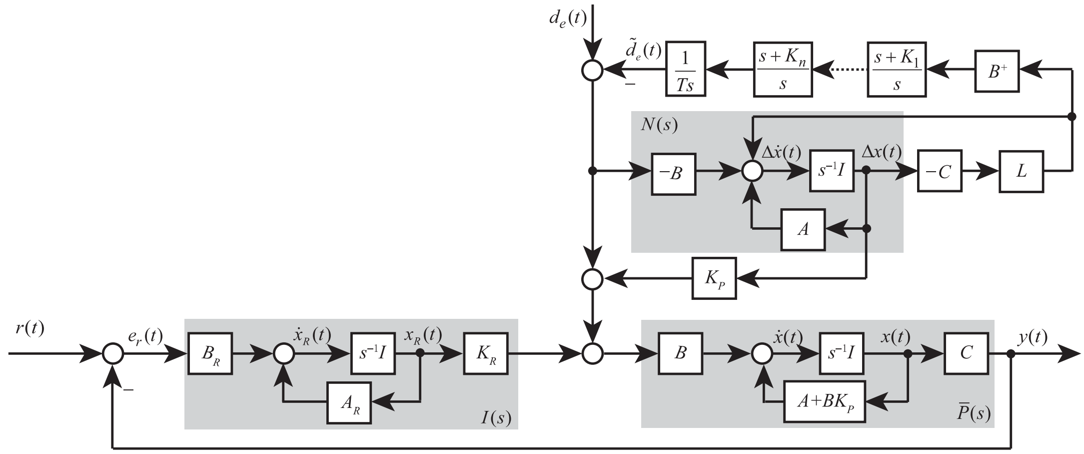

Fig. 4. Block diagram from exogenous signals to output.

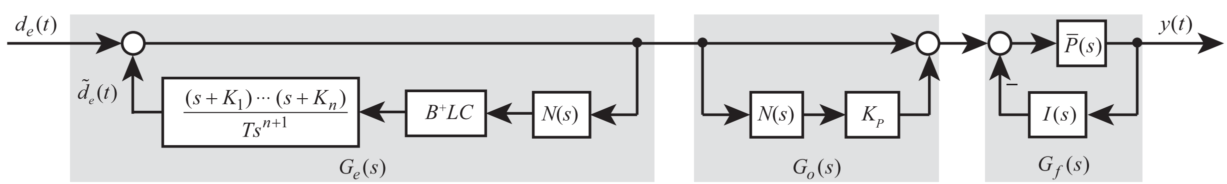

Fig. 5. Block diagram from $d_e(t)$ to $y(t)$.

The filtered $\hat{d}_e(t)$ is $\tilde{d}_e(t)$ and satisfies

$$\tilde{D}_e(s) = F(s)\hat{D}_e(s). \tag{22}$$

Incorporating $\tilde{d}_e(t)$ into the control input yields a new control law

$$u(t) = u_f(t) - \tilde{d}_e(t) \tag{23}$$

where

$$u_f(t) = [K_P\ K_R]\begin{bmatrix}\hat{x}(t)\\ x_R(t)\end{bmatrix} \tag{24}$$

and $[K_P\ K_R]$ is a feedback-gain matrix.

Remark 1: The integrals increase the indiscrimination degree of the EID estimator, which enables fast estimation dynamics of the disturbance. Moreover, since the measurement noise, $n(t)$, is a high-frequency signal, the integrals are not sensitive to it. Thus, the IEID estimator does not amplify the effect of the measurement noise.

Remark 2: Compared with the high-order DOB method [2], the IEID approach does not require all states of a plant measurable and can directly add the estimated disturbance to the input channel for compensation.

B. Stability Analysis of IEID-Based Control System

Combining (2), (3), (4), and (23) yields

$$\Delta\dot{x}(t) = (A - LC)\Delta x(t) + B[\tilde{d}_e(t) - d_e(t)]. \tag{25}$$

Combining (6), (17)–(19), and (21)–(23) yields

$$\tilde{D}_e(s) = -\frac{1}{Ts}\cdot\frac{s+K_1}{s}\cdots\frac{s+K_n}{s}B^+LC\Delta X(s). \tag{26}$$

Redrawing Fig. 3 based on (2), (4), (24), (25), and (26) yields Fig. 4, in which

$$\bar{P}(s) = C[sI - (A + BK_P)]^{-1}B \tag{27}$$

$$I(s) = K_R[sI - A_R]^{-1}B_R. \tag{28}$$

We set $r(t) = 0$ and simplify Fig. 4 to be Fig. 5, where

$$G_e(s) = \left[1 - \frac{(s+K_1)\cdots(s+K_n)}{Ts^{n+1}}B^+LCN(s)\right]^{-1} \tag{29}$$

$$G_o(s) = 1 + K_PN(s) \tag{30}$$

$$G_f(s) = \bar{P}(s)[1 + \bar{P}(s)I(s)]^{-1}. \tag{31}$$

Clearly, the transfer function from $d_e(t)$ to $y(t)$ is

$$G_{dy}(s) = G_e(s)G_o(s)G_f(s) \tag{32}$$

where $G_e(s)$, $G_o(s)$, and $G_f(s)$ are three subsystems in series. It is necessary to ensure $\|G_e\|_\infty \approx 0$ to reject the disturbance.

Since the stability is not related to exogenous signals [$r(t)$, $d(t)$, and $n(t)$], the IEID-based control system is stable if $G_e(s)$, $G_o(s)$, and $G_f(s)$ are all stable (separation theorem [26]). Thus, we should perform the following steps:

1) design the internal model, $I(s)$, and the state-feedback controller, $[K_P\ K_R]$, to ensure that $G_f(s)$ is stable;
2) design the gain of the state observer, L, to ensure that $G_o(s)$ is stable;

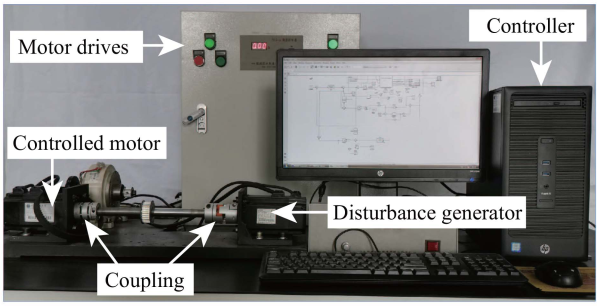

Fig. 6. Experimental setup.

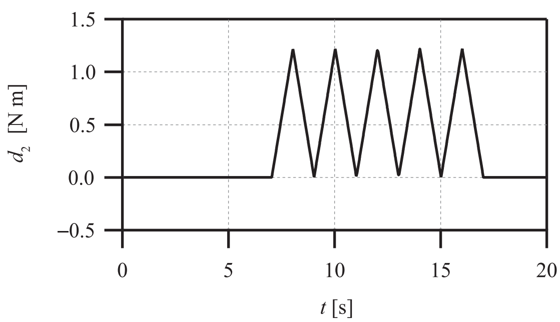

Fig. 7. Triangular disturbance.

3) design the IEID estimator [the filter, $F(s)$, and the integrals] to ensure that $G_e(s)$ is stable.

The above analysis provides the design principle of the control system, which is guaranteed in the next section.

IV. Design of IEID-Based Control System

Since the filter is designed by (7) and the state feedback controller can be easily designed using a common method (such as loop-shaping or optimal control method), we only explain the design of the internal model, the state observer, and the integrals in this section.

A. Design of State Observer

Consider the dual system of the plant (2)

$$\begin{cases} \dot{x}_d(t) = A^{\mathrm{T}} x_d(t) + C^{\mathrm{T}} u_d(t) \\ y_d(t) = B^{\mathrm{T}} x_d(t). \end{cases} \tag{33}$$

Assume that the parameterized control law is

$$u_d(t) = L_\rho^{\mathrm{T}} x_d(t) \tag{34}$$

where $\rho > 0$ is a scalar parameter. The state-feedback gain L_ρ^{T} is designed by minimizing the performance index

$$J_L = \int_0^\infty \left[\rho x_d^{\mathrm{T}}(t) Q_L x_d(t) + u_d^{\mathrm{T}}(t) R_L u_d(t)\right] \mathrm{d}t \tag{35}$$

which yields

$$L_\rho^{\mathrm{T}} = -R_L^{-1} C S \tag{36}$$

where Q_L and R_L are weighting matrices; and S is the solution of the Riccati equation

$$SA^{\mathrm{T}} + AS - SC^{\mathrm{T}} R_L^{-1} CS + \rho Q_L = 0. \tag{37}$$

Since the plant (2) is a minimum-phase system, we can obtain an L_ρ^{T}, based on the concept of perfect regulation, that ensures

$$\lim_{\rho\to\infty} [sI - (A - L_\rho C)]^{-1} B = 0. \tag{38}$$

It means that there is a large enough ρ ensuring

$$\|N\|_\infty \approx 0. \tag{39}$$

Thus, the stability of $G_o(s)$ is guaranteed according to (30).

Remark 3: Since $\|N\|_\infty \approx 0$, there is $\|G_o\|_\infty \approx 1$, that is, $G_o(s)$ has no effect on the disturbance-rejection performance.

B. Design of Integrals

According to (29), the open-loop transfer function of $G_e(s)$ is

$$G_{\mathrm{op}}(s) = -\frac{(s+K_1)\cdots(s+K_n)}{Ts^{n+1}} B^{+} LCN(s). \tag{40}$$

It can be rewritten to be

$$G_{\mathrm{op}}(s) = -\frac{(s+K_1)\cdots(s+K_n)}{Ts^{n+1}} \left[B^{+}(sI - A)N(s) - 1\right]. \tag{41}$$

Since the L designed in Section IV-A ensures $\|N\|_\infty \approx 0$, (41) can be simplified to be

$$G_{\mathrm{op}}(s) = \frac{(s+K_1)\cdots(s+K_n)}{Ts^{n+1}} \tag{42}$$

and (29) can be simplified to be

$$G_e(s) = \left[1 + \frac{(s+K_1)\cdots(s+K_n)}{Ts^{n+1}}\right]^{-1}. \tag{43}$$

According to (20) and (43), a large enough K_1 ensures a small $\|G_e\|_\infty$, that is, a well disturbance-rejection performance.

The phase-frequency characteristic of $G_{\mathrm{op}}(s)$ in (42) is

$$\varphi(\omega) = -90^\circ(n+1) + \arctan\frac{\omega}{K_1} + \cdots + \arctan\frac{\omega}{K_n}. \tag{44}$$

Its phase margin is

$$\gamma(\omega_c) = -90^\circ(n-1) + \arctan\frac{\omega_c}{K_1} + \cdots + \arctan\frac{\omega_c}{K_n} \tag{45}$$

where ω_c is the crossover frequency. Taking ω_c into (42) yields

$$\left|\frac{(j\omega_c+K_1)\cdots(j\omega_c+K_n)}{T(j\omega_c)^{n+1}}\right| = 1. \tag{46}$$

For a system, the phase margin is usually required to satisfy

$$\gamma(\omega_c) \geq 60^\circ \tag{47}$$

to guarantee the robust stability of the system. Let

$$\gamma_n(\omega_c) = -90^\circ(n-1) + n\arctan\frac{\omega_c}{K_n}. \tag{48}$$

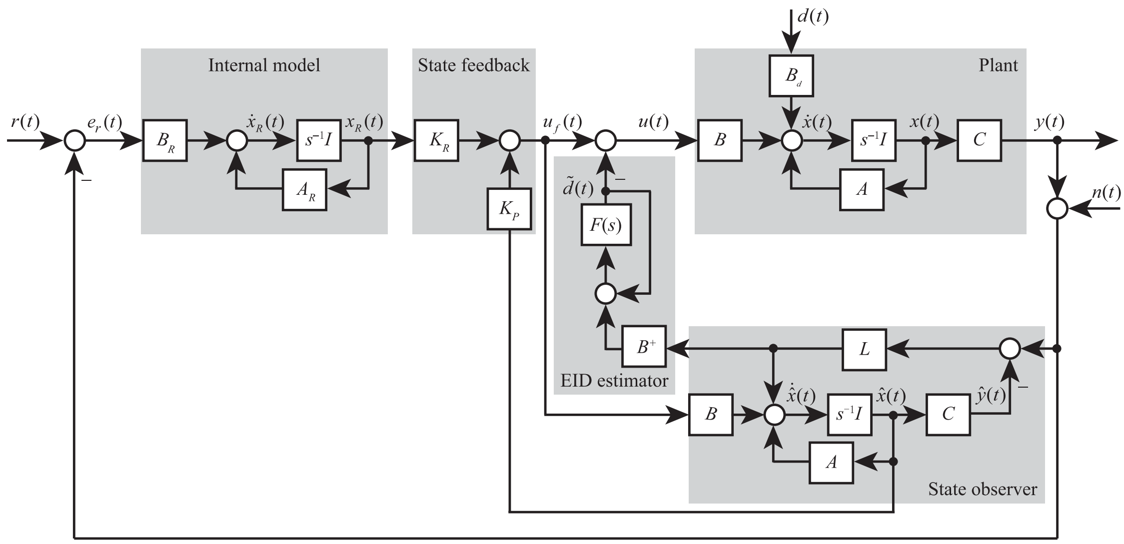

Fig. 8. Configuration of EID-based control system.

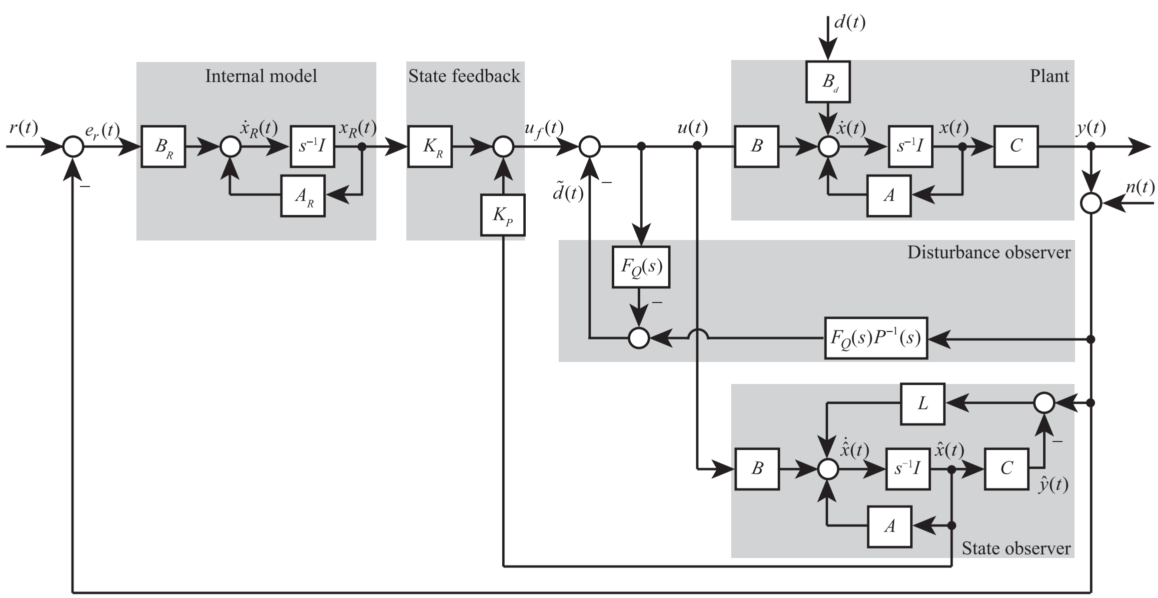

Fig. 9. Configuration of DOB-based control system.

Since $K_1 \leq K_2 \leq \cdots \leq K_n$, there is

$$\gamma(\omega_c) \geq \gamma_n(\omega_c). \tag{49}$$

Thus, if there is

$$\gamma_n(\omega_c) \geq 60^\circ \tag{50}$$

then (47) is satisfied. Substituting (48) into (50) yields

$$K_n \leq \frac{\omega_c}{\tan(\frac{3n-1}{n}30^\circ)}. \tag{51}$$

Thus, considering both the disturbance-rejection performance and the robust stability, we set the gain of the integrals to satisfy

$$K_1 = K_2 = \cdots = K_n = \frac{\omega_c}{\tan(\frac{3n-1}{n}30^\circ)}. \tag{52}$$

Then, we develop Algorithm 1 to design the integrals when the crossover frequency of the IEID estimator is limited. Combining (46) with (52) shows that ω_c increases with the increase of n. Thus, Algorithm 1 is convergent.

Remark 4: When $n = 0$, the IEID estimator is the conventional EID estimator, and (53) and (54) are true. It means that the disturbance-rejection ability of the IEID estimator designed by Algorithm 1 is better than or equal to the conventional EID estimator.

C. Design Procedure

The design steps for an IEID-based control system are as follows.

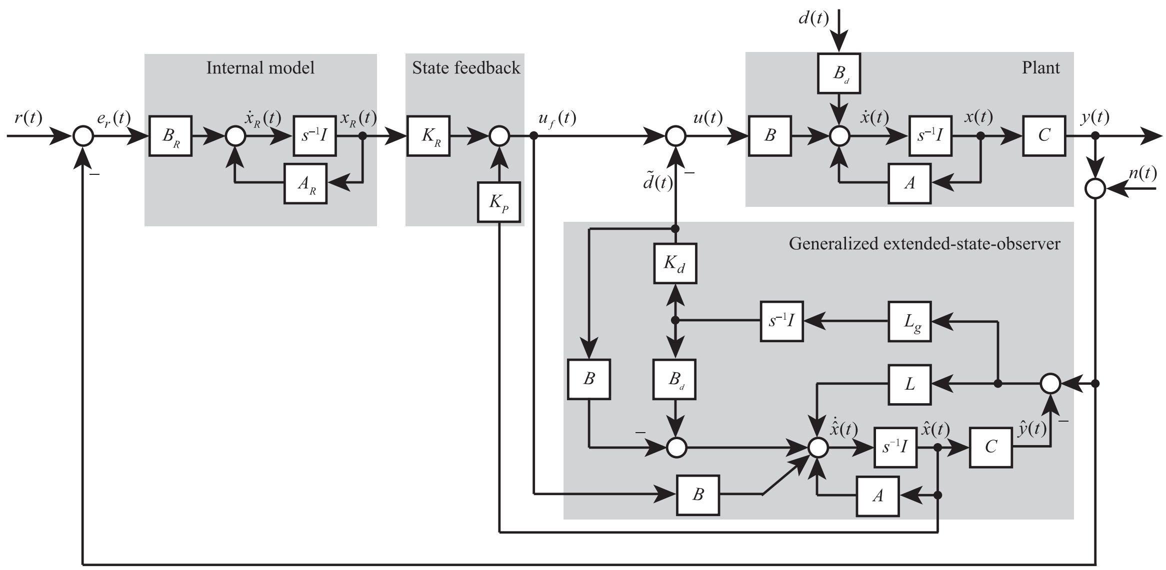

Fig. 10. Configuration of GESO-based control system.

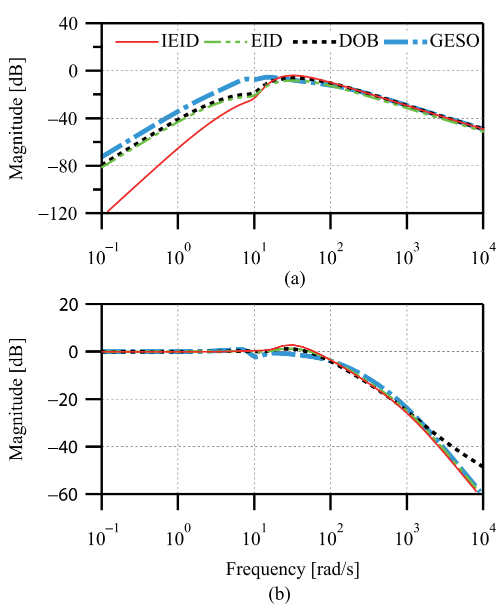

Fig. 11. Bode magnitude plots. (a) From $n(t)$ to $y(t)$. (b) From $d(t)$ to $y(t)$.

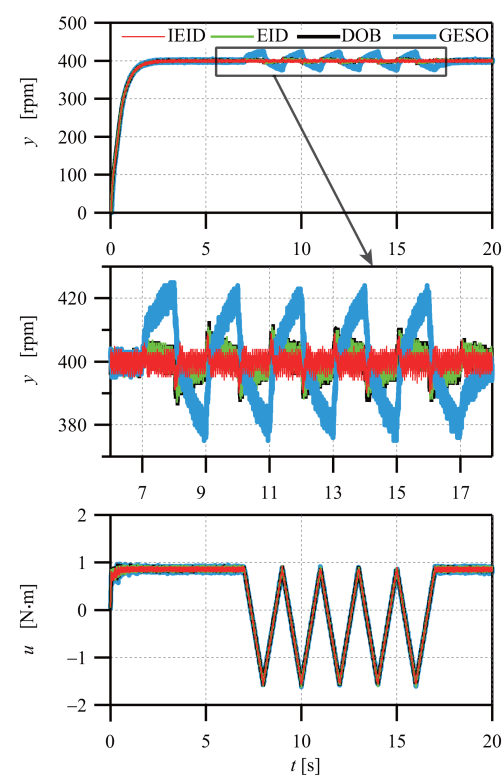

Fig. 12. Comparison results of GESO, DOB, EID, and IEID approaches in rejecting the triangular disturbance.

Step 1) Design the internal model according to the reference input $r(t)$.

Step 2) Design the feedback-gain matrix $[K_P\, K_R]$ using a common method (such as loop-shaping or optimal control method).

Step 3) Design a time constant T satisfying (6).

Step 4) Run Algorithm 1 that yields $K_1, K_2, \ldots, K_n$.

Step 5) Choose Q_L, R_L, and ρ to solve (35) that yields an $L = L_\rho$.

Step 6) Check whether (39) is true. If not, then increase ρ and go back to Step 5 until it is satisfied.

V. Experimental Verification

We used an experimental setup (Fig. 6) to verify the validity of the IEID approach. This setup mainly comprised two permanent-magnet synchronous motors (PMSMs) (ISMH1-75B30CB), two motor drives (WLK-1A III), and a controller (HP 288 Pro G2 MT). One of the PMSMs (drive motor) was

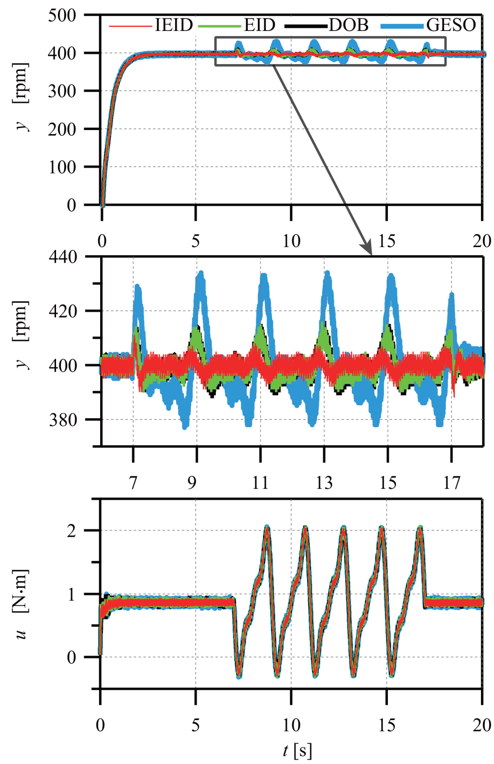

Fig. 13. Comparison results of GESO, DOB, EID, and IEID approaches in rejecting the sin disturbance.

Algorithm 1: Design of Integrals.

1: Calculate $\|G_c(j\omega)\|$ for $\omega \in [0, \omega_r]$ according to (14).
2: Set an ideal crossover frequency, $\omega_c^\star (\geq \frac{1}{T})$, for $G_{op}(s)$.
3: Set $n = 0$, $\omega_c = \frac{1}{T}$, $K_1 = K_2 = \cdots = K_n = 0$ and go to Step 6.
4: Combine (46) with (52) and calculate ω_c.
5: Take n and ω_c into (52) and calculate $K_1, K_2, \ldots, K_n$.
6: Substitute n and $K_1, K_2, \ldots, K_n$ into (43) and calculate $\|G_e(j\omega)\|$ for $\omega \in [0, \omega_r]$.
7: Check whether there are

$$\omega_c \leq \omega_c^\star \tag{53}$$

$$\|G_e(j\omega)\| \leq \|G_c(j\omega)\|. \tag{54}$$

If both (53) and (54) are true, set $\|G_c(j\omega)\| = \|G_e(j\omega)\|$ and $n = n + 1$, then go back to Step 4. Otherwise, end the algorithm.
8: Output $K_1, K_2, \ldots, K_n$.

designed to track a reference speed and another PMSM (load motor) was designed to generate a torque disturbance. The axles of the two PMSMs were coupled together. The PMSMs were equipped with 10 000 pulses/revolution optical encoders to precisely measure the rotor position. The control program was implemented using MATLAB/Simulink under TwinCAT 3, and the sampling time was 0.0005 s. The parameters of the PMSMs are shown in Table I, where $j = p, d$ represents the drive motor and the load motor, respectively. The dynamic model of the drive

TABLE I
PARAMETERS OF THE PMSMS

Parameter	Meaning	Unit
τ_j	Torque produced	$\mathrm{N \cdot m}$
τ_{pd}	Twisting torque	$\mathrm{N \cdot m}$
ω_j	Rotational speed	rad/s
θ_j	Rotation angle	rad
J_j	Inertia	$\mathrm{kg \cdot m^2}$
B_{mj}	Viscous damping coefficient	$\mathrm{N \cdot m \cdot s}$
K_{pd}	Twisting elasticity coefficient of coupling	$\mathrm{N \cdot m}$

motor is

$$J_p \dot{\omega}_p(t) = \tau_p(t) - \tau_{pd}(t) - B_{mp}\omega_p(t). \tag{55}$$

And that of the load motor is

$$J_d \dot{\omega}_d(t) = \tau_d(t) + \tau_{pd}(t) - B_{md}\omega_d(t) \tag{56}$$

where $\tau_{pd}(t) = K_{pd}[\theta_p(t) - \theta_d(t)]$.

Let $x_p(t) = [\omega_p(t)\, \omega_d(t)\, \theta_p(t) - \theta_d(t)]$, $u(t) = \tau_p(t)$, $d(t) = \tau_d(t)$, and $y_p(t) = \omega_p(t)$. Then, the state-space equation of the setup can be rewritten as the form of the plant (1) and its parameters were identified to be

$$\begin{cases} A = \begin{bmatrix} -5.132 & 0 & -101.2 \\ 0 & -5.132 & 101.2 \\ 1 & -1 & 0 \end{bmatrix} & B = \begin{bmatrix} 34.04 \\ 0 \\ 0 \end{bmatrix} \\ B_d = \begin{bmatrix} 0 & 34.04 & 0 \end{bmatrix}^{\mathrm{T}} & C = \begin{bmatrix} 1 & 0 & 0 \end{bmatrix}. \end{cases} \tag{57}$$

Simple verification shows that this system satisfies Assumptions 1 2.

A. Design of Control System

First, consider tracking a step reference input

$$r(t) = 400 \times 1(t) \text{ r/min}. \tag{58}$$

Its internal model is

$$A_R = 0,\ B_R = 1. \tag{59}$$

We used the linear-quadratic-regulator method to design the feedback-gain matrix $[K_P\ K_R]$. A state-space model containing the plant (2) and the internal model of $r(t)$ is

$$\begin{bmatrix} \dot{x}(t) \\ \dot{x}_R(t) \end{bmatrix} = \begin{bmatrix} A & 0 \\ -B_R C & A_R \end{bmatrix} \begin{bmatrix} x(t) \\ x_R(t) \end{bmatrix} + \begin{bmatrix} B \\ 0 \end{bmatrix} u(t). \tag{60}$$

Minimizing the performance index

$$J_K = \int_0^\infty \left\{ \begin{bmatrix} x(t) \\ x_R(t) \end{bmatrix}^{\mathrm{T}} Q_K \begin{bmatrix} x(t) \\ x_R(t) \end{bmatrix} + u^{\mathrm{T}}(t) R_K u(t) \right\} \mathrm{d}t$$

where the weighting matrices were chosen to be

$$Q_K = \mathrm{diag}\,\{1,\ 1,\ 1,\ 10\},\ R_K = 1$$

yielded

$$K_P = [1.001 \quad 0.1440 \quad 2.353],\ K_R = -3.162. \tag{61}$$

TABLE II
COMPARISON RESULTS OF GESO, DOB, EID, AND IEID APPROACHES

Disturbance	Approach		Index: IAE		ITAE		ISE		ITSE		PPV	
Sawtooth	GESO	$\frac{\text{IEID}}{\text{GESO}} \times 100\%$	120.0	15.22%	1555	15.25%	1822	3.08%	23529	3.10%	50	38%
	DOB	$\frac{\text{IEID}}{\text{DOB}} \times 100\%$	36.29	50.32%	473.6	50.06%	181.7	30.89%	2375	30.67%	25	76%
	EID	$\frac{\text{IEID}}{\text{EID}} \times 100\%$	36.00	50.72%	470.1	50.43%	179.2	31.32%	2344	31.07%	24	79%
	IEID		18.26		237.1		56.12		728.3		19	
Sine	GESO	$\frac{\text{IEID}}{\text{GESO}} \times 100\%$	106.2	18.15%	1378	17.97%	1779	3.37%	23030	3.27%	57	37%
	DOB	$\frac{\text{IEID}}{\text{DOB}} \times 100\%$	36.92	52.22%	480.6	51.52%	224.7	26.70%	2929	25.74%	26	81%
	EID	$\frac{\text{IEID}}{\text{EID}} \times 100\%$	36.63	52.63%	476.6	51.95%	221.2	27.12%	2882	26.16%	26	81%
	IEID		19.28		247.6		59.99		753.9		21	

Next, consider rejecting two types of disturbances. One is a sine disturbance containing a basic frequency and two harmonics

$$d_1(t) = 0.4\sin \pi t + 0.2 \sin 2\pi t + 0.1 \sin 3\pi t \, \mathrm{N{\cdot}m}. \tag{62}$$

Another is a triangular disturbance (Fig. 7), which containing infinite harmonics. Since the highest angular frequency for the $d_1(t)$ is $\omega_r = 3\pi$ rad/s, we designed the time constant of the filter to be $T = 0.03$ s according to (7). We set the ideal crossover frequency to be $\omega_c^\star = 30$ rad/s and ran Algorithm 1, which yielded

$$n = 1, \, K_1 = 17.32.$$

Then, choose $\rho = 10^6$ and the weighting matrices of (35) to be

$$Q_L = [1 \, 10^{-6} \, 10^{-6}], \, R_L = 1.$$

Minimizing the performance index, J_L, yielded

$$L = [994.8 \; -0.002982 \; 0.9700]^{\mathrm{T}}$$

and $\|N\|_\infty = 0.03404$ satisfying (39).

B. Experiments and Comparisons

A comparison between the IEID approach with the conventional EID approach (Fig. 8), the DOB approach (Fig. 9), and the GESO approach (Fig. 10) was carried out. The parameters (A_R, B_R, K_R, K_P, and L) of those approaches were set to be same as the IEID approach. For comparing with the EID approach [7], we set the filter of the EID approach to be $F(s) = \frac{1}{0.03s+1}$. For comparing with the DOB approach [27], we constructed an inverse model $P^{-1}(s)$ of the system (57), and a filter $F_Q(s) = \frac{1}{0.03s+1}$ to implement $P^{-1}(s)$ for the DOB approach. For comparing with the GESO approach [28], we designed $K_d = 1.791$ according to [5] and set $L_g = 538.3$ to make $B^+L/0.03 = K_d L_g$ according to [28].

For analyzing the disturbance-rejection performance of the three approaches, we gave the Bode magnitude plots of the closed-loop transfer functions from $d(t)$ to $y(t)$ [Fig. 11(a)]. Since the magnitude of the IEID approach is the smallest for $\omega \in [0, \, 3\pi]$, its disturbance-rejection performance is the best. The Bode magnitude plots from the measurement noise, $n(t)$, to $y(t)$ [Fig. 11(b)] shows that the IEID approach, the EID approach, and the GESO approach have the same magnitudes and are smaller than that of the DOB approach for the high-frequency band. Thus, the noise-suppression ability of the IEID approach, the EID approach, and the GESO approach are better than that of the DOB approach.

In the experiments, we added the step reference input, $r(t)$, to the GESO-, DOB-, EID-, and IEID-approach-based control systems when $t \geq 0$ s. Since the four control systems include the internal model of $r(t)$, all of them track it without steady-state error when there is no disturbance (Figs. 12 and 13). After the systems entered the steady state, we added the disturbances to the systems during $7 \sim 17$ s. Experimental results show that the IEID approach is much better than EID and DOB approaches in rejecting triangular and sine disturbances while the control inputs of the approaches are similar (Figs. 12 and 13).

To further compare the four approaches, we calculated the peak-to-peak value (PPV), integral absolute error (IAE), integral time absolute error (ITAE), integral square error (ISE), and integral time square error (ITSE) of the tracking error:

$$\begin{cases} \text{IAE} = \int_7^{17} |e_r(t)|\mathrm{d}t, \; \text{ITAE} = \int_7^{17} t|e_r(t)|\mathrm{d}t \\ \text{ISE} = \int_7^{17} e_r^2(t)\mathrm{d}t, \; \text{ITSE} = \int_7^{17} te_r^2(t)\mathrm{d}t. \end{cases} \tag{63}$$

The comparison results (Table II) show that those indexes of the IEID approach are smaller than that of the EID, DOB, and GESO approaches when rejecting the triangular and sine disturbances. It means that the IEID approach has a great improvement in rejecting exogenous disturbances.

VI. CONCLUSION

In this article, we embedded integrals to the conventional EID estimator that developed an IEID approach. The IEID approach improved the disturbance-rejection performance for a plant without amplifying the effect of measurement noise. The validity of the approach was demonstrated through a rotational speed control system. Experiments showed that the approach is superior to the GESO approach, the DOB approach, and the conventional EID approach.

Note that this study considered a single-input and single-output system. However, the IEID approach can handle multiinput and multioutput systems. This will be carried out in the future.

REFERENCES

[1] Z. Gao, "On the centrality of disturbance rejection in automatic control," *ISA Trans.*, vol. 53, no. 4, pp. 850–857, Jul. 2014.

[2] K. Kim, K. Rew, and S. Kim, "Disturbance observer for estimating higher order disturbances in time series expansion," *IEEE Trans. Autom. Control*, vol. 55, no. 8, pp. 1905–1911, Aug. 2010.

[3] E. Sariyildiz, R. Oboe, and K. Ohnishi, "Disturbance observer-based robust control and its applications: 35th anniversary overview," *IEEE Trans. Ind. Electron.*, vol. 67, no. 3, pp. 2042–2053, Mar. 2020.

[4] J. Han, "From PID to active disturbance rejection control," *IEEE Trans. Ind. Electron.*, vol. 56, no. 3, pp. 900–906, Mar. 2009.

[5] S. Li, J. Yang, W. Chen, and X. Chen, "Generalized extended state observer based control for systems with mismatched uncertainties," *IEEE Trans. Ind. Electron.*, vol. 59, no. 12, pp. 792–4802, Dec. 2012.

[6] W. Chen, J. Yang, L. Guo, and S. Li, "Disturbance observer-based control and related methods: An overview," *IEEE Trans. Ind. Electron.*, vol. 63, no. 2, pp. 1083–1095, Feb. 2016.

[7] J. She, M. Fang, Y. Ohyama, H. Hashimoto, and M. Wu, "Improving disturbance-rejection performance based on an equivalent-input-disturbance approach," *IEEE Trans. Ind. Electron.*, vol. 55, no. 1, pp. 380–389, Jan. 2008.

[8] J. She, X. Xin, and Y. Pan, "Equivalent-input-disturbance approach-analysis and application to disturbance rejection in dual-stage feed drive control system," *IEEE/ASME Trans. Mechatron.*, vol. 16, no. 2, pp. 330–340, Apr. 2011.

[9] Z. Wang, J. She, Z. Liu, and M. Wu, "Modified equivalent-input-disturbance approach to improving disturbance-rejection performance," *IEEE Trans. Ind. Electron.*, vol. 69, no. 1, pp. 673–683, Jan. 2022.

[10] Q. Mei, J. She, and Z. Liu, "Disturbance rejection and control system design based on a high-order equivalent-input-disturbance estimator," *J. Franklin Inst.*, vol. 358, no. 16, pp. 8736–8753, Oct. 2021.

[11] P. Yu, M. Wu, J. She, K. Liu, and Y. Nakanishi, "Robust tracking and disturbance rejection for linear uncertain system with unknown state delay and disturbance," *IEEE/ASME Trans. Mechatron.*, vol. 23, no. 3, pp. 1445–1455, Jun. 2018.

[12] P. Yu, K. Liu, X. Liu, X. Li, M. Wu, and J. She, "Analysis of equivalent-input-disturbance-based control systems and a coordinated design algorithm for uncertain systems," *Int. J. Robust Nonlinear Control.*, vol. 31, no. 5, pp. 1755–1773, Mar. 2021.

[13] Y. Du, W. Cao, J. She, M. Wu, M. Fang, and S. Kawata, "Disturbance rejection for input-delay system using observer-predictor-based output feedback control," *IEEE Trans. Ind. Informat.*, vol. 16, no. 7, pp. 4489–4497, Jul. 2020.

[14] X. Wu, J. She, L. Yu, H. Dong, and W. Zhang, "Contour tracking control of networked motion control system using improved equivalent-input-disturbance approach," *IEEE Trans. Ind. Electron.*, vol. 68, no. 6, pp. 5155–5165, Jun. 2021.

[15] X. Yin, J. She, M. Wu, D. Sato, and K. Hirota, "Disturbance rejection and performance analysis for nonlinear systems based on nonlinear equivalent-input-disturbance approach," *Nonlinear Dyn.*, vol. 100, no. 5, pp. 3497–3511, May 2020.

[16] X. Yin, J. She, Z. Liu, M. Wu, D. Sato, and K. Hirota, "Chaos suppression in speed control for permanent-magnet-synchronous-motor drive system," *J. Franklin Inst.*, vol. 357, no. 18, pp. 13283–13303, Dec. 2020.

[17] Q. Mei, J. She, Z. Liu, and M. Wu, "Estimation and compensation of periodic disturbance using internal-model-based equivalent-input-disturbance approach," *Sci. China Inf. Sci.*, vol. 64, no. 7, pp. 1–14, Mar. 2021. doi: 10.1007/s11432-020-3192-5.

[18] W. Cai, J. She, M. Wu, and Y. Ohyama, "Disturbance suppression for quadrotor UAV using sliding-mode-observer-based equivalent-input-disturbance approach," *ISA Trans.*, vol. 92, no. 9, pp. 286–297, Sep. 2019.

[19] M. Wu, F. Gao, P. Yu, J. She, and W. Cao, "Improve disturbance-rejection performance for an equivalent-input-disturbance-based control system by incorporating a proportional-integral observer," *IEEE Trans. Ind. Electron.*, vol. 67, no. 2, pp. 1254–1260, Feb. 2020.

[20] Y. Du, W. Cao, J. She, M. Wu, and M. Fang, "Disturbance rejection via feedforward compensation using an enhanced equivalent-input-disturbance approach," *J. Franklin Inst.*, vol. 357, no. 15, pp. 10977–10996, Oct. 2021.

[21] Q. Mei, J. She, F. Wang, Y. Nakanishi, H. Hashimoto, and D. Chugo, "Disturbance rejection and control system design using 1-inverse-based equivalent-input-disturbance approach," *IEEE Trans. Ind. Electron*., 2022, to be published, doi: 10.1109/TIE.2022.3161805.

[22] P. Yu, M. Wu, J. She, K. Liu, and Y. Nakanishi, "An improved equivalent-input-disturbance approach for repetitive control system with state delay and disturbance," *IEEE Trans. Ind. Electron.*, vol. 65, no. 1, pp. 521–531, Jan. 2018.

[23] Z. Wang, J. She, and G. Wang, "Adaptive equivalent-input-disturbance approach to improving disturbance-rejection performance," *Int. J. Control Autom.*, vol. 17, no. 5, pp. 701–712, May. 2020.

[24] Y. Du, W. Cao, J. She, M. Wu, M. Fang, and S. Kawata, "Disturbance rejection and control system design using improved equivalent input disturbance approach," *IEEE Trans. Ind. Electron.*, vol. 67, no. 4, pp. 3013–3023, Apr. 2020.

[25] L. R. Hunt, G. Meyer, and R. Su, "Noncausal inverses for linear systems," *IEEE Trans. Autom. Control*, vol. 41, no. 4, pp. 608–611, Apr. 1996.

[26] B. D. O. Anderson and J. B. Moore, *Optimal Control-Linear Quadratic Methods*. Englewood Cliffs, NJ, USA: Prentice-Hall, 1989.

[27] E. Schrijver and J. van Dijk, "Disturbance observers for rigid mechanical systems: Equivalence, stability, and design," *J. Dyn. Syst. Meas. Control*, vol. 124, pp. 539–548, Dec. 2002.

[28] P. Yu, K. Liu, J. She, M. Wu, and Y. Nakanishi, "Robust disturbance rejection for repetitive control systems with time-varying nonlinearities," *Int. J. Robust Nonlinear Control.*, vol. 29, no. 5, pp. 1597–1612, Mar. 2019.

Qicheng Mei received the M.S. degree in control engineering from the China University of Geosciences, Wuhan, China, in 2018. He is currently working toward the Ph.D. degree in control science and engineering from the China University of Geosciences.

His research interests include the disturbance estimation and rejection, application of control theory, and robust control.

Jinhua She (Fellow, IEEE) received the B.S. degree in engineering from Central South University, Changsha, China, in 1983, and the M.S. and Ph.D. degrees in engineering from the Tokyo Institute of Technology, Tokyo, Japan, in 1990 and 1993, respectively.

Since 1993, he has been a Professor with the School of Engineering, Tokyo University of Technology. His research interests include the application of control theory, repetitive control, process control, mobile education, and assistive robotics.

Dr. She was a recipient of the IFAC (International Federation of Automatic Control) Control Engineering Practice Prize Paper Award in 1999 (jointly with M. Wu and M. Nakano). He is also a Member of the Society of Instrument and Control Engineers, the Institute of Electrical Engineers of Japan, the Japan Society of Mechanical Engineers, and the Asian Control Association.

Feng Wang (Member, IEEE) received the Ph.D. degree in computer science from Central South University, Changsha, China, in 2018.

From 2019 to 2021, he was an Overseas Researcher (JSPS Fellow) with the School of Engineering, Tokyo University of Technology, Tokyo, Japan. He is currently an Associate Professor with the School of Automation, China University of Geosciences, Wuhan, China. His research interests include social network analysis, machine learning, IoT, and recommendation systems.

Yosuke Nakanishi (Member, IEEE) received the B.S. and M.S. degrees in electrical engineering from Waseda University, Shinjuku-ku, Japan, in 1978 and 1980, respectively, and the Ph.D. degree in electrical engineering from Tokyo Metropolitan University, Hachioji, Japan, in 1996.

In 1980, he joined Fuji Electric Company. After starting his career in the R&D section, he has mainly dedicated himself to power system analysis work as well as development of power system simulators and engineering programs for monitoring control systems. He is currently a Professor with the Graduate School of Environment and Energy Engineering, Waseda University, Tokyo, Japan. His research interests include simulation and analysis of power systems and distribution power systems.

Dr. Nakanishi was the recipient of a Prize Paper Award from the IEEE Power Engineering Education Committee in 1991. He is a Senior Member of the IEE, Tokyo, Japan, a Member of the CIGRE, Paris, France, a Convenor of the Investigation Committee on Grid Technologies for large amount of Wind Power, and a Member of the Investigation Committee on History of Power System Analysis, both at IEEJ, Tokyo, Japan.